

# 1 The Silicon Vertex Detector of the Belle II Experiment

2 Y. Uematsu<sup>a</sup>, K. Adamczyk<sup>t</sup>, L. Aggarwal<sup>l</sup>, H. Aihara<sup>q</sup>, T. Aziz<sup>j</sup>, S. Bacher<sup>t</sup>,  
3 S. Bahinipati<sup>f</sup>, G. Batignani<sup>k,l</sup>, J. Baudot<sup>e</sup>, P. K. Behera<sup>g</sup>, S. Bettarini<sup>k,l</sup>,  
4 T. Bilka<sup>c</sup>, A. Bozek<sup>t</sup>, F. Buchsteiner<sup>b</sup>, G. Casarosa<sup>k,l</sup>, L. Corona<sup>k,l</sup>, T. Czank<sup>p</sup>,  
5 S. B. Das<sup>h</sup>, G. Dujany<sup>e</sup>, C. Finck<sup>e</sup>, F. Forti<sup>k,l</sup>, M. Friedl<sup>b</sup>, A. Gabrielli<sup>m,n</sup>,  
6 E. Ganiev<sup>m,n</sup>, B. Gobbo<sup>n</sup>, S. Halder<sup>j</sup>, K. Hara<sup>r,o</sup>, S. Hazra<sup>j</sup>, T. Higuchi<sup>p</sup>,  
7 C. Irmeler<sup>b</sup>, A. Ishikawa<sup>r,o</sup>, H. B. Jeon<sup>s</sup>, Y. Jin<sup>m,n</sup>, C. Joo<sup>p</sup>, M. Kaleta<sup>t</sup>,  
8 A. B. Kaliyar<sup>j</sup>, J. Kandra<sup>c</sup>, K. H. Kang<sup>s</sup>, P. Kapusta<sup>t</sup>, P. Kodyš<sup>c</sup>, T. Kohriki<sup>r</sup>,  
9 M. Kumar<sup>h</sup>, R. Kumar<sup>i</sup>, C. La Licata<sup>p</sup>, K. Lalwani<sup>h</sup>, R. Le Boucher<sup>d</sup>,  
10 S. C. Lee<sup>s</sup>, J. Libby<sup>g</sup>, L. Martel<sup>e</sup>, L. Massacesi<sup>k,l</sup>, S. N. Mayekar<sup>j</sup>,  
11 G. B. Mohanty<sup>j</sup>, T. Morii<sup>p</sup>, K. R. Nakamura<sup>r,o</sup>, Z. Natkaniec<sup>t</sup>, Y. Onuki<sup>q</sup>,  
12 W. Ostrowicz<sup>t</sup>, A. Paladino<sup>k,l</sup>, E. Paoloni<sup>k,l</sup>, H. Park<sup>s</sup>, G. Polat<sup>d</sup>, K. K. Rao<sup>j</sup>,  
13 I. Ripp-Baudot<sup>e</sup>, G. Rizzo<sup>k,l</sup>, D. Sahoo<sup>j</sup>, C. Schwanda<sup>b</sup>, J. Serrano<sup>d</sup>,  
14 J. Suzuki<sup>r</sup>, S. Tanaka<sup>r,o</sup>, H. Tanigawa<sup>q</sup>, R. Thalmeier<sup>b</sup>, R. Tiwari<sup>j</sup>,  
15 T. Tsuboyama<sup>r,o</sup>, O. Verbycka<sup>t</sup>, L. Vitale<sup>m,n</sup>, K. Wan<sup>q</sup>, Z. Wang<sup>q</sup>, J. Webb<sup>a</sup>,  
16 J. Wiechczynski<sup>l</sup>, H. Yin<sup>b</sup>, L. Zani<sup>d</sup>,

17 (Belle-II SVD Collaboration)

18 <sup>a</sup>*School of Physics, University of Melbourne, Melbourne, Victoria 3010, Australia*

19 <sup>b</sup>*Institute of High Energy Physics, Austrian Academy of Sciences, 1050 Vienna, Austria*

20 <sup>c</sup>*Faculty of Mathematics and Physics, Charles University, 121 16 Prague, Czech Republic*

21 <sup>d</sup>*Aix Marseille Université, CNRS/IN2P3, CPPM, 13288 Marseille, France*

22 <sup>e</sup>*IPHC, UMR 7178, Université de Strasbourg, CNRS, 67037 Strasbourg, France*

23 <sup>f</sup>*Indian Institute of Technology Bhubaneswar, Satya Nagar, India*

24 <sup>g</sup>*Indian Institute of Technology Madras, Chennai 600036, India*

25 <sup>h</sup>*Malaviya National Institute of Technology Jaipur, Jaipur 302017, India*

26 <sup>i</sup>*Punjab Agricultural University, Ludhiana 141004, India*

27 <sup>j</sup>*Tata Institute of Fundamental Research, Mumbai 400005, India*

28 <sup>k</sup>*Dipartimento di Fisica, Università di Pisa, I-56127 Pisa, Italy*

29 <sup>l</sup>*INFN Sezione di Pisa, I-56127 Pisa, Italy*

30 <sup>m</sup>*Dipartimento di Fisica, Università di Trieste, I-34127 Trieste, Italy*

31 <sup>n</sup>*INFN Sezione di Trieste, I-34127 Trieste, Italy*

32 <sup>o</sup>*The Graduate University for Advanced Studies (SOKENDAI), Hayama 240-0193, Japan*

33 <sup>p</sup>*Kavli Institute for the Physics and Mathematics of the Universe (WPI), University of*

34 *Tokyo, Kashiwa 277-8583, Japan*

35 <sup>q</sup>*Department of Physics, University of Tokyo, Tokyo 113-0033, Japan*

36 <sup>r</sup>*High Energy Accelerator Research Organization (KEK), Tsukuba 305-0801, Japan*

37 <sup>s</sup>*Department of Physics, Kyungpook National University, Daegu 41566, Korea*

38 <sup>t</sup>*H. Niewodniczanski Institute of Nuclear Physics, Krakow 31-342, Poland*

---

## 39 Abstract

40 The Silicon Vertex Detector (SVD) is a part of the vertex detector in the  
41 Belle II experiment at the SuperKEKB collider (KEK, Japan). Since the start  
42 of data taking in spring 2019, the SVD has been operating stably and reliably

43 with a high signal-to-noise ratio and hit efficiency, achieving good spatial resolu-  
44 tion and high track reconstruction efficiency. The hit occupancy, which mostly  
45 comes from the beam-related background, is currently about 0.5% in the in-  
46 nermost layer, causing no impact on the SVD performance. In anticipation of  
47 the operation at higher luminosity in the next years, two strategies to sustain  
48 the tracking performance in future high beam background conditions have been  
49 developed and tested on data. One is to reduce the number of signal waveform  
50 samples to decrease dead time, data size, and occupancy. The other is to utilize  
51 the good hit-time resolution to reject the beam background hits. We also mea-  
52 sured the radiation effects on the sensor current, strip noise, and full depletion  
53 voltage caused during the first two and a half years of operation. The results  
54 show no detrimental effect on the SVD performance.

55 *Keywords:* Silicon strip detector, Vertex detector, Tracking detector, Belle II

---

## 56 1. Introduction

57 The Belle II experiment [1] aims to probe new physics beyond the Standard  
58 Model in high-luminosity  $e^+e^-$  collisions at the SuperKEKB collider (KEK,  
59 Japan) [2]. SuperKEKB consists of the following components: injector LINAC,  
60 positron damping ring, and main storage ring with the electron and positron  
61 beamlines. The Belle II detector is located at the interaction point (IP) of  
62 the two beamlines. The main collision energy in the center-of-mass system is  
63 10.58 GeV on the  $\Upsilon(4S)$  resonance, which enables various physics programs  
64 based on the large samples of B mesons,  $\tau$  leptons, and D mesons. Also, the  
65 asymmetric energy of the 7 GeV electron beam and 4 GeV positron beam is  
66 adopted for time-dependent  $CP$  violation measurements. The target of Su-  
67 perKEKB is to accumulate an integrated luminosity of  $50 \text{ ab}^{-1}$  with peak lu-  
68 minosity of about  $6 \times 10^{35} \text{ cm}^{-2}\text{s}^{-1}$ . In June 2021, SuperKEKB recorded the  
69 world's highest instantaneous luminosity of  $3.1 \times 10^{34} \text{ cm}^{-2}\text{s}^{-1}$ . The data accu-  
70 mulated before July 2021 corresponds to an integrated luminosity of  $213 \text{ fb}^{-1}$ .

71 The Vertex Detector (VXD) is the innermost detector in the Belle II detector

72 system. The VXD has six layers: the inner two layers (layers 1 and 2) are the  
 73 Pixel Detector (PXD), and the outer four layers (layers 3 to 6) are the Silicon  
 74 Vertex Detector (SVD). The schematic cross-sectional view of the VXD is shown  
 75 in Fig. 1. The PXD consists of DEPFET pixel sensors, and its innermost radius  
 76 is 1.4 cm from the IP. A detailed description of the SVD appears in Sec. 2.

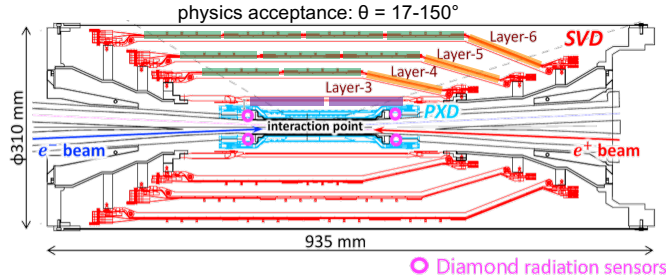


Figure 1: Schematic cross-sectional view of the VXD. The SVD is in red, the PXD is in light blue, and the IP beam pipe diamonds are in pink circles. In the upper half of the VXD the locations of the three types of SVD DSSDs are indicated by boxes in three colors: purple for small sensors, green for large sensors, and orange for trapezoidal sensors as described in Tab. 1.

77 Diamond sensors [3], used to monitor the radiation dose and for the beam  
 78 abort system, are mounted on the IP beam pipe and the bellows pipes outside of  
 79 the VXD. The pink circles in Fig. 1 indicate the locations of the diamond sensors  
 80 on the IP beam pipe. The diamond’s measured doses are used to estimate  
 81 the dose in the SVD. The diamond system also sends beam abort requests to  
 82 SuperKEKB if the radiation level gets too high to avoid severe damage to the  
 83 detector.

## 84 2. Belle II Silicon Vertex Detector

85 The SVD is crucial for extrapolating the tracks to the PXD. This task is  
 86 essential for measuring the decay vertices with the PXD and pointing at a region-  
 87 of-interest limiting the PXD readout data volume. Other roles of the SVD are  
 88 the standalone track reconstruction of low-momentum charged particles and

89 their particle identification using ionization energy deposits. The SVD also  
 90 plays a critical role in the decay vertex measurement in the case of long-lived  
 91 particles like  $K_S$  mesons, which decay inside the SVD volume.

92 The SVD [4] consists of four layers of double-sided silicon strip detectors  
 93 (DSSDs). The material budget of the SVD is about 0.7% of a radiation length  
 94 per layer. On each DSSD plane, a local coordinate is defined with  $u$  and  $v$ :  
 95  $u$ -axis along n-side strips and  $v$ -axis perpendicular to  $u$ -axis. In other words,  
 96 p-side strips and n-side strips provide  $u$  and  $v$  information, respectively. In the  
 97 cylindrical coordinate,  $u$  corresponds to  $r-\varphi$  information and  $v$  corresponds to  
 98  $z$  information. The SVD consists of three types of sensors: “small” rectangular  
 99 sensors in layer 3, “large” rectangular sensors in the barrel region of layers 4, 5,  
 100 and 6, and “trapezoidal” sensors in the forward region of layers 4, 5, and 6, which  
 101 is slanted. They are indicated by purple, green, and orange boxes in Fig. 1. The  
 102 main characteristics of these three types of sensors are summarized in Tab. 1.  
 103 The sensors are manufactured by two companies: the small and large sensors  
 104 by Hamamatsu and trapezoidal sensors by Micron. The full depletion voltage is  
 105 60 V for Hamamatsu sensors and 20 V for Micron sensors; both types of sensors  
 106 are operated at 100 V. In total, 172 sensors are assembled, corresponding to a  
 107 total sensor area of 1.2 m<sup>2</sup> and approximately 224,000 readout strips.

	Small	Large	Trapezoidal
No. of u/p-strips	768	768	768
u/p-strip pitch	50 $\mu\text{m}$	75 $\mu\text{m}$	50–75 $\mu\text{m}$
No. of v/n-strips	768	512	512
v/n-strip pitch	160 $\mu\text{m}$	240 $\mu\text{m}$	240 $\mu\text{m}$
Thickness	320 $\mu\text{m}$	320 $\mu\text{m}$	300 $\mu\text{m}$
Manufacturer	Hamamatsu		Micron

Table 1: Table of the main characteristics of the three types of sensors. Only readout strips are taken into account for number of strips and strip pitch. All sensors have one intermediate floating strip between two readout strips.

108 Sensor strips are AC coupled to the front-end ASIC, the APV25 [5], which

109 was originally developed for the CMS Silicon Tracker. The APV25 tolerates  
110 more than 100 Mrad of radiation. It has 128 channels with a shaping time of  
111 about 50 ns. For the SVD, the APV25 is operated in “multi-peak” mode. The  
112 mechanism of the data sampling in the multi-peak mode is explained in Fig. 2.  
113 The chip samples the height of the signal waveform with the 32 MHz clock (31 ns  
114 period) and stores each sample’s information in an analog ring buffer. Since  
115 the bunch-crossing frequency is eight times faster than the sampling clock, the  
116 stored samples are not synchronous to the beam collision, in contrast to CMS,  
117 which motivates operation in the multi-peak mode. In the present readout  
118 configuration (the six-samples mode), at every reception of the Belle II global  
119 Level-1 trigger, the chip reads out six successive samples of the signal waveform  
120 stored in the buffers. The six-samples mode offers a wide enough time window  
121 ( $6 \times 31 \text{ ns} = 187 \text{ ns}$ ) to accommodate large timing shifts of the trigger. In  
122 preparation for operation with higher luminosity, where background occupancy,  
123 trigger dead-time, and the data size increase, we developed the three/six-mixed  
124 acquisition mode (mixed-mode). The mixed-mode is a new method to read out  
125 the signal samples from the APV25, in which the number of the samples changes  
126 between three and six in each event, depending on the timing precision of each  
127 Level-1 trigger signal in that event. For triggers with good timing precision,  
128 three-samples data are read out and the data have half time window and half  
129 data size compared to ones of six-samples data, resulting in the reduction of the  
130 effects due to higher luminosity. This functionality was already implemented  
131 in the running system and confirmed by a few hours of smooth physics data  
132 taking. Before we start to use the mixed-mode, the effect on the performance  
133 due to the change of the acquisition mode is to be assessed. As the first step,  
134 the effect in the hit efficiency was evaluated as described in Sec. 3.

135 The APV25 chips are mounted on each middle sensor (chip-on-sensor con-  
136 cept) with thermal isolation foam in between. The merit of this concept is  
137 shorter signal propagation length, leading to smaller capacitance of the signal  
138 line and hence reduced noise level. To minimize the material budget the APV25  
139 chips on the sensor are thinned down to 100  $\mu\text{m}$ . The APV25 chips are mounted

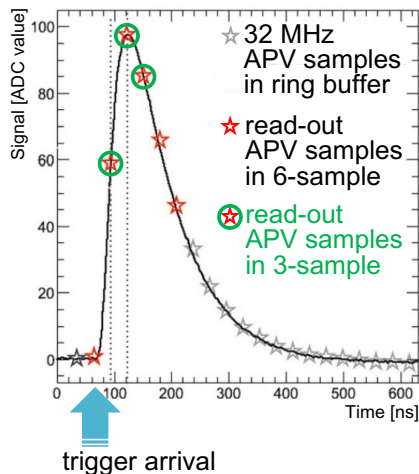


Figure 2: Example of sampling in “multi-peak” mode of the APV25. The black line shows the signal waveform after the CR-RC shaper circuit. The stars show the sampled signal height recorded in the analog ring buffer according to the 32 MHz sampling clock. The red stars indicate the six successive samples read out at the trigger reception in the six-samples mode. The red stars with a green circle indicate the samples read out in the three-samples acquisition.

140 on a single side of the sensor and readout of the signals from the opposite side  
 141 is performed via wrapped flexible printed circuits. The power consumption of  
 142 the APV25 chip is 0.4 W/chip and in total 700 W in the entire SVD. The chips  
 143 are cooled by a bi-phase  $-20^{\circ}\text{C}$   $\text{CO}_2$  evaporative cooling system.

### 144 3. Performance

145 The SVD was combined with the PXD to complete the VXD assembly in  
 146 October 2018, and the VXD was installed to the Belle II detector system in  
 147 November 2018. Since March 2019, the SVD has been operating reliably and  
 148 smoothly for two and a half years. The total fraction of masked strips is about  
 149 1%. There was only one issue where one APV25 chip (out of 1,748 chips) was  
 150 disabled during the spring of 2019, which was remediated by reconnecting a  
 151 cable in the summer of 2019.

152 The SVD has also demonstrated stable and excellent performance [6]. The

153 hit efficiency is continuously over 99% in most of the sensors. The cluster  
154 charge distributions are also reasonable. On the u/p-side, the most probable  
155 values agree with the calculated charge amount induced by MIPs within the  
156 uncertainty in calibration. On the v/n-side, 10–30% of the collected charge is  
157 lost compared to the signal collected on the u/p-side, due to the presence of the  
158 floating strip combined with the large pitch on the v/n-side. The most probable  
159 values of the cluster signal-to-noise ratio distributions range from 13 to 30.

160 We measured the cluster position resolution by analyzing the  $e^+e^- \rightarrow \mu^+\mu^-$   
161 data [7]. The cluster position resolution is estimated from the residual between  
162 the cluster position and the track position, not biased by the target cluster,  
163 after subtracting the effect of the track extrapolation error. The cluster posi-  
164 tion resolutions for different incident angles are shown in Fig. 3. The observed  
165 resolution has the expected shape, showing a minimum at the incident angle for  
166 which the projection of the track along the direction perpendicular to the strips  
167 on the detector plane corresponds to two strip pitches. Given the various sensor  
168 pitches with one floating strip, the minimum is expected at 14 (21) degrees on  
169 the v/n-side and at 4 (7) degrees on the u/p-side, respectively for layer 3 (4, 5,  
170 and 6). The resolution for normal incident angle is also in good agreement with  
171 the expected digital resolution, that is 23 (35)  $\mu\text{m}$  on the v/n-side, 7 (11)  $\mu\text{m}$   
172 on the u/p-side, respectively for layer 3 (4, 5, and 6). Still, some studies are on-  
173 going to improve the analysis for the cluster resolution especially for the layer-3  
174 u/p-side, where at normal incidence a slightly higher resolution is measured  
175 (9  $\mu\text{m}$ ) compared to the expectations .

176 The cluster hit-time resolution was also evaluated in candidate hadronic  
177 events<sup>1</sup> using the reference event time estimated by the Central Drift Chamber  
178 (CDC) outside of the SVD. The error on the event time, about 0.7 ns, was  
179 subtracted to evaluate the intrinsic SVD hit-time resolution. The resulting  
180 resolution is 2.9 ns on the u/p-side and 2.4 ns on the v/n-side. With such  
181 precise hit-time information, it is possible to reject off-time background hits

---

<sup>1</sup>The events with more than three good tracks and not like Bhabha scattering.

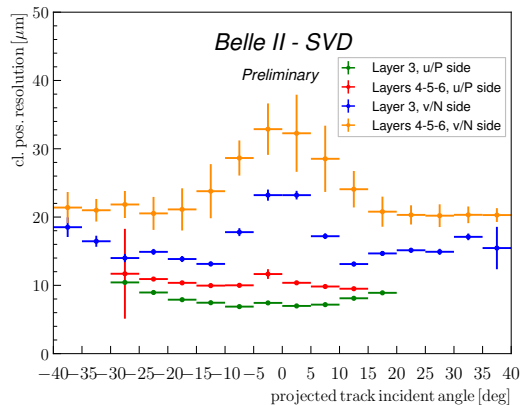


Figure 3: The SVD cluster position resolution depending on the projected track incident angle. The green (blue) plot shows the resolution in the u/p-side (n/v-side) of layer-3 sensors, and the red (yellow) one shows the u/p-side (n/v-side) of layers-4, 5, and 6 sensors.

182 efficiently. The hit-time distributions for signal<sup>2</sup> and background<sup>3</sup> are shown  
 183 in Fig. 4. The signal distribution has a narrow peak, while the background  
 184 hit-time distribution is broad and almost flat in the signal peak region. The  
 185 separation power of the hit-time is high, as expected. For example, if we reject  
 186 hits with the hit-time less than  $-38$  ns in this plot, we can reject 45% of the  
 187 background hits while keeping 99% of the signal hits. The background rejection  
 188 based on the hit-time is essential to sustain the good tracking performance in  
 189 the future high beam background condition.

190 The performance in three-samples data was compared with that in six-  
 191 samples data to evaluate the performance in the mixed-mode. If the trigger  
 192 timing has no deviation, the three-samples data will show comparable perfor-  
 193 mance to the six-samples data because the relevant part of the signal waveform  
 194 to evaluate the necessary signal properties, i.e., the signal height and the signal  
 195 timing, can be accommodated in the three-sample's time window. However,  
 196 when the trigger has a jitter and the timing shift happens, some part of the

<sup>2</sup>The clusters found to be used in the tracks in the hadronic events.

<sup>3</sup>The clusters in events triggered by delayed-Bhabha pseudo-random trigger.



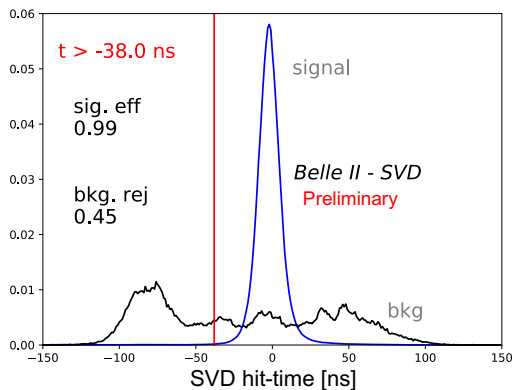


Figure 4: Example of the background hit rejection using hit-time. The blue distribution shows the signal, and the black distribution shows the background. Assuming the hit-time cut at  $-38$  ns, the signal hit efficiency of 99% and the background hit rejection of 45% are achieved.

197 signal waveform can be out of the three-sample's time window, and the recon-  
 198 struction performance deteriorates. We examined the effect on the hit efficiency  
 199 as a function of the trigger timing shift. The effect is evaluated by the rel-  
 200 ative hit efficiency, which is defined as the ratio of the hit efficiency in the  
 201 three-samples data to the one in the six-samples data. For this study, the three-  
 202 samples data are emulated in the offline analysis from the six-samples data by  
 203 selecting consecutive three samples at a fixed latency with respect to the Level-  
 204 1 trigger signal. The trigger timing shift is evaluated by the CDC event time.  
 205 The resulting relative efficiencies as a function of the trigger timing shift in the  
 206 hadronic events are shown in Fig. 5. The decreasing trend is observed for the  
 207 shift of the trigger timing, as expected. As a result, the relative efficiency is  
 208 over 99.9% for the trigger timing shift within  $\pm 30$  ns, which is almost all the  
 209 events.

#### 210 4. Beam-related background effects on SVD

211 The beam-related background increases the hit occupancy of the SVD, which  
 212 in turn degrades the tracking performance. Considering this performance degra-  
 213 dation, we set the occupancy limit in layer-3 sensors to be about 3%, which will

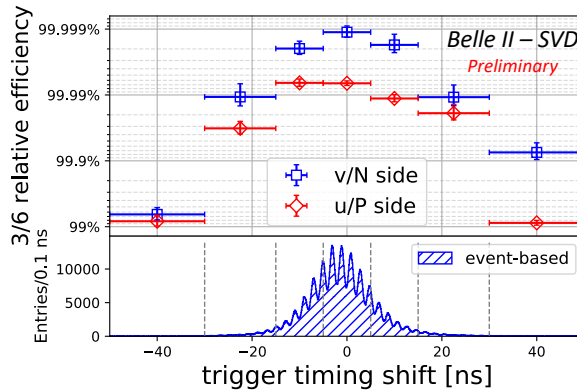


Figure 5: The relative hit efficiencies (the ratios of the hit efficiency in the three-samples data to the one in the six-samples data) as a function of the trigger timing shift for v/n-side (blue square) and u/p-side (red diamond). The positive (negative) trigger timing shift corresponds to early (late) trigger timing.

214 be loosened roughly by a factor of two after we apply the hit-time rejection  
 215 described in Sec. 3. With the current luminosity, the average hit occupancy in  
 216 layer-3 sensors is less than 0.5%. However, the projection of the hit occupancy  
 217 at the luminosity of  $8 \times 10^{35} \text{ cm}^{-2}\text{s}^{-1}$  is about 3% in layer-3 sensors. The  
 218 projected occupancy comes from the Monte Carlo (MC) simulation scaled by  
 219 the data/MC ratio determined from the beam background data of the current  
 220 beam optics. The corresponding integrated dose, using the data/MC-rescaled  
 221 beam background extrapolation, is about 0.2 Mrad/smy, and the equivalent 1-  
 222 MeV neutron fluence is about  $5 \times 10^{11} \text{ n}_{\text{eq}}/\text{cm}^2/\text{smy}$  (smy: Snowmass Year =  
 223  $10^7$  sec). Considering the radiation hardness of the SVD sensors, about 10 Mrad  
 224 and about  $10^{13} \text{ n}_{\text{eq}}/\text{cm}^2$ , based on the experience of similar DSSD sensors used  
 225 in the BaBar Silicon Vertex Tracker [8], we expect to be able to safely operate  
 226 the SVD even for ten years at high luminosity, with some safety margin with  
 227 respect to beam background extrapolation of about a factor two to three. The  
 228 long-term extrapolation of the beam background is affected by large uncertain-  
 229 ties from the optimization of collimator settings in MC and the future evolution  
 230 of the beam injection background, which is not simulated. This uncertainty,

231 together with the relatively small safety factor two to three between the beam  
232 background extrapolation and the detector limits, motivates the VXD upgrade  
233 which improves the tolerance of the hit rates and the radiation damage, and the  
234 technology assessment is ongoing for multiple sensor options.

235 In the first two and a half years of operation the integrated radiation dose  
236 in the layer-3 mid-plane sensors, which are the most exposed in the SVD, is  
237 estimated to be 70 krad. The estimation is based on the measured dose by the  
238 diamonds on the beam pipe exploiting the measured correlation between the  
239 SVD occupancy and the diamond dose [9]. Thanks to the introduction of a new  
240 random trigger line, recently made available, we could improve the dose analysis,  
241 removing a bias of about a factor 3 that gave an overestimation of the dose in  
242 the previous analysis. The new estimate still has an uncertainty of about 50%,  
243 mainly due to the unavailability of the appropriate trigger before December  
244 2020. Assuming the dose/ $n_{\text{eq}}$  fluence ratio of  $2.3 \times 10^9$   $n_{\text{eq}}/\text{cm}^2/\text{krad}$  from MC,  
245 1-MeV equivalent neutron fluence is evaluated to be about  $1.6 \times 10^{11}$   $n_{\text{eq}}/\text{cm}^2$   
246 in the first two and a half years.

247 The effect of the integrated dose on the sensor leakage current is measured,  
248 and the results show a clear linear correlation as in the upper plot of Fig. 6. The  
249 slopes for all the sensors are 2–5  $\mu\text{A}/\text{cm}^2/\text{Mrad}$ , as summarized in the lower  
250 plot of Fig. 6. The large variations can be explained by temperature effects and  
251 the deviation of sensor-by-sensor dose from the average in each layer used in  
252 the estimation. The slopes are in the same order of magnitude as previously  
253 measured in the BaBar experiment [8], 1  $\mu\text{A}/\text{cm}^2/\text{Mrad}$  at 20°C. The precise  
254 temperature in layer 3 of the SVD is unknown, but expected to be in a similar  
255 regime. While the leakage current is increasing, the impact on the strip noise  
256 is suppressed by the short shaping time (50 ns) in APV25. It is expected to be  
257 comparable to the strip-capacitive noise only after 10 Mrad irradiation and not  
258 problematic for ten years where the integrated dose is estimated to be 2 Mrad.

259 The evolution of the noise with the integrated dose is shown in Fig. 7. The  
260 noise increase of 20–25% is observed in layer 3, but this does not affect the  
261 SVD performance. This noise increase is likely due to the radiation effects on

262 the sensor surface. Fixed oxide charges on sensor surface increase with dose,  
263 with some saturation expected at around 100 krad, enlarging also non-linearly  
264 the inter-strip capacitance, also expected to saturate with dose. The noise  
265 saturation is already observed on the v/n-side and also starts to be seen on the  
266 u/p-side.

267 The full depletion voltage of the sensor is also a key property that can be  
268 affected by the radiation damage. It can be measured from the v/n-side strip  
269 noise, which suddenly decreases at the full depletion voltage because the sensor  
270 substrate is n-type and thus the v/n-side strips are only fully isolated at full  
271 depletion. From this measurement full depletion voltages consistent with mea-  
272 surements performed on the bare sensors before the installation were obtained,  
273 ranging from 20 to 60 V, and so far no change in full depletion voltage is ob-  
274 served in the first two and a half years of operation, which is consistent with  
275 the expectation from low integrated neutron fluence of  $1.6 \times 10^{11} \text{ n}_{\text{eq}}/\text{cm}^2$ .

## 276 5. Conclusions

277 The SVD has been taking data in Belle II since March 2019 smoothly and  
278 reliably. The detector performance is excellent and agrees with expectations.  
279 We are ready to cope with the increased background during higher luminosity  
280 running by rejecting the off-time background hits using hit-time and operating  
281 in the three/six-mixed acquisition mode. In the recent study, the efficiency  
282 loss in the three-samples data is confirmed to be less than 0.1% for the trigger  
283 timing shift within  $\pm 30$  ns. The observed first effects of radiation damage are  
284 also within expectation and do not affect the detector performance.

## 285 Acknowledgments

286 This project has received funding from the European Union's Horizon 2020  
287 research and innovation programme under the Marie Skłodowska-Curie grant  
288 agreements No 644294 and 822070. This work is supported by MEXT, WPI,  
289 and JSPS (Japan); ARC (Australia); BMBWF (Austria); MSMT (Czechia);

290 CNRS/IN2P3 (France); AIDA-2020 (Germany); DAE and DST (India); INFN  
291 (Italy); NRF and RSRI (Korea); and MNiSW (Poland).

## 292 **References**

- 293 [1] T. Abe, et al., Belle II Technical Design Report (2010). arXiv:1011.0352.
- 294 [2] Y. Ohnishi, et al., Accelerator design at SuperKEKB, Prog. Theor. Exp.  
295 Phys. 2013 (3), 03A011 (03 2013).
- 296 [3] S. Bacher, et al., Performance of the diamond-based beam-loss monitor sys-  
297 tem of Belle II, Nucl. Instrum. Methods Phys. Res., Sect. A 997 (2021)  
298 165157. arXiv:2102.04800.
- 299 [4] K. Adamczyk, et al., The Belle II silicon vertex detector assembly and me-  
300 chanics, Nucl. Instrum. Methods Phys. Res., Sect. A 845 (2017) 38–42, pro-  
301 ceedings of the Vienna Conference on Instrumentation 2016.
- 302 [5] M. J. French, et al., Design and results from the APV25, a deep sub-micron  
303 CMOS front-end chip for the CMS tracker, Nucl. Instrum. Methods Phys.  
304 Res., Sect. A 466 (2001) 359–365.
- 305 [6] G. Rizzo, et al., The Belle II Silicon Vertex Detector: Performance and  
306 Operational Experience in the First Year of Data Taking, JPS Conf. Proc.  
307 34, 010003 (2021).
- 308 [7] R. L. Boucher, et al., Measurement of the cluster position resolution of the  
309 Belle II Silicon Vertex Detector, these NIMA Conference Proceedings.
- 310 [8] B. Aubert, et al., The BaBar detector: Upgrades, operation and perfor-  
311 mance, Nucl. Instrum. Methods Phys. Res., Sect. A 729 (2013) 615–701.
- 312 [9] L. Massaccesi, Performance study of the SVD detector of Belle II and future  
313 upgrades, master thesis, Dipartimento di Fisica *E. Fermi*, Università di  
314 Pisa (2021).  
315 URL <https://docs.belle2.org/record/2759/>

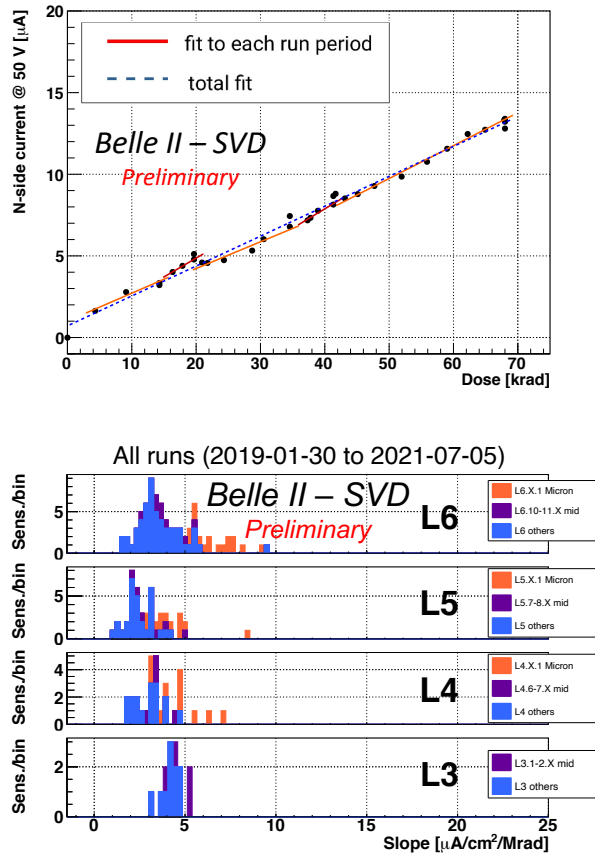


Figure 6: (upper) Effect of the integrated dose on the leakage current in the n/v-side of one layer-3 sensor. The slope is fitted for each run period (solid red line) and all the runs (dashed blue line). Both fit results agree with each other and are consistent with the linear increase. (lower) The fit results of all the sensors for all runs. The sensors are classified as trapezoidal sensors in the forward region (Micron), sensors around the midplane, and the others.

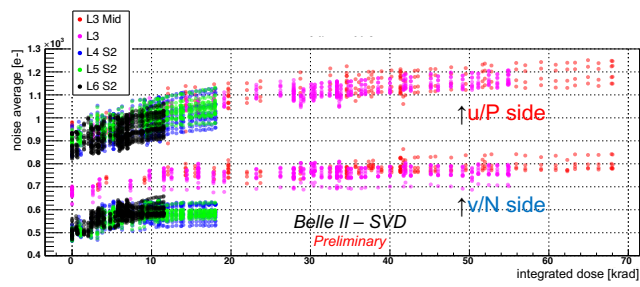


Figure 7: Effect of the integrated dose on the noise average in electron. The clear increase is observed and saturated (or start to be saturated) for layer-3 sensors.